Eur. Phys. J. D **44**, 283–288 (2007)
DOI: 10.1140/epjd/e2007-00181-x

THE EUROPEAN PHYSICAL JOURNAL D

Laser-plasma interaction in the context of inertial fusion: experiments and modeling

C. Labaune[1,a], K. Lewis[1,2], H. Bandulet[1], S. Depierreux[2], S. Hüller[3], P.E. Masson-Laborde[2,3], D. Pesme[3], and P. Loiseau[2]

[1] Laboratoire pour l'Utilisation des Lasers Intenses, École Polytechnique / CNRS, 91128 Palaiseau, France
[2] CEA-DIF, B.P. 12, 91680 Bruyères-Le-Châtel, France
[3] Centre de Physique Théorique, CNRS, École Polytechnique, 91128 Palaiseau, France

Received 15 June 2006 / Received in final form 11 May 2007
Published online 6 June 2007 –

Abstract. Many nonlinear processes may affect the laser beam propagation and the laser energy deposition in the underdense plasma surrounding the pellet. These processes, associated with anomalous and nonlinear absorption mechanisms, are fundamental issues in the context of Inertial Confinement Fusion. The work presented in this article refers to laser-plasma interaction experiments which were conducted under well-controlled conditions, and to their theoretical and numerical modeling. Thanks to important diagnostics improvements, the plasma and laser parameters were sufficiently characterized in these experiments to make it possible to carry out numerical simulations modeling the laser plasma interaction in which the hydrodynamics conditions were very close to the experimental ones. Two sets of experiments were carried out with the LULI 2000 and the six beam LULI laser facilities. In the first series of experiments, the interaction between two single hot spots was studied as a function of their distance, intensity and light polarization. In the second series, the intensity distribution of stimulated Brillouin scattering (SBS) inside the plasma was studied by means of a new temporally resolved imaging system. Two-dimensional (2D) simulations were carried out with our code Harmony2D in order to model these experiments. For both series of experiments, the numerical results show a very good agreement with the experimental ones for what concerns the main SBS features, namely the spatial and temporal behavior of the SBS-driven acoustic waves, as well as the average SBS reflectivities. Thus, these well diagnosed experiments, carried out with well defined conditions, make it possible to benchmark our theoretical and numerical modelings and, hence, to improve our predictive capabilities for future experiments.

PACS. 52.38.-r Laser-plasma interactions – 52.38.Bv Rayleigh scattering; stimulated Brillouin and Raman scattering – 52.65.-y Plasma simulation – 52.70.Kz Optical (ultraviolet, visible, infrared) measurements

1 Introduction

Many nonlinear processes [1] can affect the propagation and the coupling of the laser beams with the underdense plasma surrounding the laser fusion pellet. Among them, filamentation and self-focusing [2] may modify the laser intensity distribution, and eventually lead to beam spreading. In addition, the parametric scattering instabilities, Stimulated Brillouin Scattering (SBS) and Stimulated Raman Scattering (SRS), are able to induce energy losses, to modify the angular distribution of the laser light, and to generate high energy electrons. These instabilities are of primary importance for laser fusion, because they may significantly reduce the laser absorption efficiency and uniformity in ignition scale targets [3]. The potential risk in neglecting these processes was impressively demonstrated by recent experiments carried out at the National Ignition Facility (NIF) with laser and plasma parameters close to the future laser fusion experiments: SBS reflectivities of the order of 30% were measured during the main (high intensity) laser pulse, eventually leading to a proportional decrease of the radiation temperature of the "indirect-drive" hohlraum target [4]. Controlling the nonlinear processes responsible for these detrimental consequences is therefore a primary issue and requires a good physical understanding and adequate modeling capabilities.

Much progress on the understanding of these nonlinear processes has been achieved in the last few years, thanks to coordinated efforts between experiments, theory and numerical simulations.

On the experimental side, multiple beam experiments made it possible to create and to probe well-controlled and well-characterized plasmas, independently of the "interaction beam". This progress resulted from a flexible

[a] e-mail: kristin@greco2.polytechnique.fr

laser beam geometry and timing. In middle size facilities, sophisticated experiments, with many complementary diagnostics, have been carried out with a large number of laser shots, thus allowing the complete characterization of the plasma parameters.

On the basis of such well-prepared experiments, realistic plasma temperature and density profiles have been deduced from the diagnostics and from accompanying hydrodynamical simulations. These profiles have then been introduced in the numerical simulations describing the main laser-plasma interaction, bringing the simulations and the experiments closer each one to the other. In addition, new numerical diagnostics, mimicking the experimental ones, have been developed [5].

Two techniques have been used in the experiments presented in this paper, so as to have a well-defined laser intensity distribution in the focal volume. In the first series of experiments, described in Section 2, a special focusing device was designed so as to give rise to two single, well defined hot spots in the focal volume. Such a case can easily be modeled numerically. The second series of experiments, presented in Section 3, was carried out with the use of random phase plates (RPP), which is a technique able to produce a well-defined speckle distribution in vacuum in the focal plane [6]. Such a RPP beam can be adequately modeled theoretically and simulated numerically.

2 Interaction between two laser 'hot spots'

In this section, we present new experimental results in which the interaction of two neighboring laser beams in a plasma was investigated. This experiment was designed in order to mimic the interaction of two neighboring laser speckles of a RPP beam. The two neighboring hot spots configuration was obtained by using a diaphragm on the laser beam so as to use only a small part of the transverse section; thus, the phase front can be considered to be flat, which allows to focus each beam to a limit close to the diffraction limit.

In so-called "single hot spot" experiments, the volume of the interacting plasma is limited and can nowadays be easily described numerically. Thus, such single hot spot experiments, well diagnosed and carried out under well defined conditions, are particularly useful to make progress in laser-plasma interaction physics: indeed, on one hand, they are able to provide data from a reduced-scale interaction region with high spatial and temporal resolutions [7], and with a good knowledge of the intensity and (!) phase of the laser field; on the other hand, they can be modeled and numerically simulated, making it possible to benchmark the numerical codes. Moreover, the single hot spots experiments are useful to understand the fundamental physical mechanisms taking place in multiple hot spot configurations, such as in RPP beams. In particular, the question of the independence of individual hot spots with respect to the laser-plasma interaction remains a primary issue. Indeed, in numerous models involving parametric instabilities, the independence of individual laser speckles is assumed [8] a priori. Thus, the backscatter-reflectivities due to SBS and/or SRS have mainly been computed within this hypothesis [9]. On the other hand, as discussed in reference [10], several mechanisms are able to make the speckles to interact between them. Two types of coupling between speckles may occur: (i) on the fast time scale, an electromagnetic coupling can take place due to the propagation of the diffracted and scattered light by each of the speckles; (ii) on the slow (acoustic) time scale, a hydrodynamic coupling can occur, associated with ion density perturbations propagating between the speckles. Thus, it remains important to find out experimentally whether the hot spots can be considered to be independent or not for what concerns laser-plasma interaction.

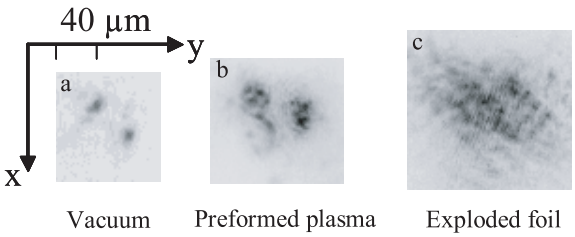

Fig. 1. Images of the intensity distribution at best focus as a function of the coordinates x and y transverse to the laser propagation axis: (a) in vacuum; (b) in a preformed plasma; (c) in a thin exploded foil.

We set-up an experiment using the LULI 2000 facility designed to study the effect on the light propagation of a second hot spot in the close neighborhood of a first hot spot. More specifically, this experiment consisted in splitting a coherent laser beam into two sub-beams, in focusing these two sub-beams in a plasma, so that the mutual distance, relative intensities, and polarization of the two resulting speckles were well defined, and in qualifying the laser light propagation features as a function of these parameters and of the electron plasma density.

The energy of each of the two main laser LULI 2000 beams was 400 J at 0.53 μm, in a 1.5 ns square pulses, and they were separated in angle by 45°. The first beam, the "plasma formation beam", was focused through a $f/4$ lens with a RPP on a thin plastic foil in order to preform the plasma by exploding the foil. The second beam, the "interaction beam", was delayed by 1.5 ns and was focused through a pair of holes covered by small prisms and a $F = 800$ mm corrected lens in order to produce the two sub-beams. The holes were 50 mm in diameter, when the diameter of the laser beam was 200 mm. The phase plane of the beam was almost flat for such a transverse distance, and indeed we could observe two neighboring hot spots in the focal volume in vacuum as shown in Figure 1a. The size of each hot spot was 17 μm in diameter (zero to zero) and 10 μm at full width at half maximum (FWHM). The maximum intensity, corresponding to full laser energy, was 1.5×10^{16} W/cm^2; however, most of the shots were done with a reduced energy. The main diagnostics were based on images of the intensity distribution in the plane transverse to the propagation direction. These images were taken inside the plasma, where the best focus was found in the plasma-free case. Two

types of imaging were designed: (1) "snapshots" of the 2D transverse cross section of the beam, with a temporal integration over about 100 ps; (2) one single transverse direction (1D) as a function of time. The domain over which the images were taken around the best focus had a spatial width of 10 μm (in the propagation direction), i.e. it was small as compared with the single hot spot Rayleigh length $L_R \sim$ 400 μm.

In a first part of these experiments, we compared the laser intensity distribution in the following three cases: the case "a" corresponds to the shots with no target, so that the imaging was made inside vacuum; the case "b" corresponds to the experiments when the formation beam was fired 1.5 ns before the interaction beam on the thin foil. Although the target is a thin foil, this case "b" will be referred to, in the following, as the "preformed plasma" case, for simplicity, because the hydrodynamics plasma parameters evolve slowly when the interaction beam hits the target; the case "c" corresponds to the experiments made when the formation beam was not used, so that the interaction beam interacted directly with the thin foil target. This case "c" will be referred to as the "thin foil" case. The distance between the two hot spots in vacuum (case "a") was 40 μm. Obviously, they do not overlap at best focus, as shown in Figure 1a. In the preformed plasma case ("b") at the time of arrival of the interaction beam, the density profile was quasi-parabolic along the laser axis, with a plasma density below quarter critical during the interaction pulse. From hydrodynamic simulations, we could estimate the electron temperature in the range $T_e = 0.5$–0.7 keV and the ion temperature in the range $T_i = 0.2$–0.4 keV. It can be observed in Figure 1b that each hot spot is fragmented, although remaining well separated from the other. The hot spot fragmentation can be interpreted as due to filamentation. For $n_e/n_c \sim 0.2$ and $T_e = 0.7$ keV, the critical power for filamentation is $P_c \sim 0.1$ GW, whereas the laser beam power is $P_L \sim 0.1 I_{14}$ GW, I_{14} denoting the laser intensity in units of 10^{14} W/cm^2. Therefore, the criterion for the onset of self-focusing, namely $p > 1$, with $p \equiv P_L/P_c \sim I_{14}$ is well satisfied in the intensity regime $I > 10^{14}$ W/cm^2 considered here.

We now consider with more details the preformed plasma case ("b") for which the plasma conditions are well-defined. The most significant result can be seen by comparing the temporally resolved images, shown in Figure 2, of the intensity distribution in one dimension transverse to the laser axis. Figure 2a shows the case "a" of a single hot spot, and Figure 2b shows the case "b" of two neighboring hot spots separated by a well-defined distance, denoted as d. The hot spot distance corresponding to Figure 2b is $d = 20$ μm. The images were taken in the center of the plasma inside the hot spot(s). In Figure 2a, where only a single beam is present, the onset of filamentation is evidenced by the occurrence of several parallel, and almost stationary streaks in the x-direction. In the case of two neighboring hot spots, Figure 2b, the image is completely different as compared to Figure 2a, in that the image does not show features which could be clearly related to individual hot spots, even if each of them were

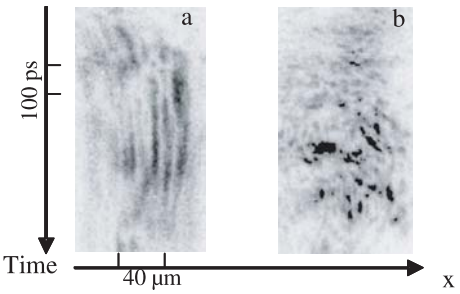

Fig. 2. Time-resolved intensity distribution inside the plasma as a function of one of the transverse coordinates, x. Case (a) of a single hot spot; (b) in the presence of a second hot spot, the distance between the hot spots being $d = 20$ μm.

in a self-focusing stage. Indeed, the image exhibits a very non-stationary behavior of the transverse laser intensity profile with transient high intensity peaks corresponding to short lifetime filaments, and the initial location of each hot spot cannot be identified in this turbulent stage. Thus, the image of Figure 2b rather indicates that some global process is taking place, involving the two hot spots together. Therefore, we interpret the image of Figure 2b as demonstrating that the two hot spots strongly interact one with each other.

In order to confirm this interpretation, we now put some estimates concerning the possibility for two hot spots to interact between them. A simple estimate of the hydrodynamic interaction time between two parallel hot spots, $t_{hyd} \sim d/c_s$ leads to a value of the order 60–80 ps. which is shorter than the time interval 100 ps shown on the left hand side of Figure 2 (c_s denotes the plasma sound velocity; c_s is of the order of $c_s \sim 0.2$–0.25 μm/ps for the case considered here). Thus, the time scale of the experiment, as well as the time interval corresponding to Figure 2, is sufficiently long to make it possible to observe the interaction between the two hot spots, if an hydrodynamic-type coupling was effectively taking place between them. We also have to consider the effect of the ion acoustic wave (IAW) damping on the density perturbation during their propagation from one hot spot to the other. Indeed, the ion acoustic wave (IAW) damping, denoted as ν_{iaw}, is able to attenuate the density perturbations emitted from the first hot spot before they reach the second one [10] whenever the inequality $\nu_{iaw} d/c_s > 1$ is satisfied. Consequently, the coupling between neighboring hot spots is expected to be negligible whenever the condition $\nu_{iaw} d/c_s > 1$ is fulfilled [11]. The damping ν_{iaw} can be obtained from the value of the ratio ν_{iaw}/ω_{iaw} characterizing the IAWs, where $\omega_{iaw} \equiv k c_s$ stands for the frequency of the IAW perturbation with wavenumber k. The wavenumbers k of the IAW perturbations produced by one hot spot typically satisfy the inequality $k > \pi/D$, where D denotes the hot spot diameter and can be estimated to twice the beam waist a_0, namely $D \approx 2a_0 = 12$ μm [where a_0 is related by the factor $1/2(\ln 2)^{1/2}$ with the beam diameter at FWHM, being 10 μm as indicated earlier]. From the inequalities $\nu_{iaw} d/c_s > 1$ and $k > \pi/D$, one deduces that the inequality $d/D > [\pi \nu_{iaw}/\omega_{iaw}]^{-1}$ is a *sufficient*

condition that ensures that the two neighboring hot spots do not interact. More precisely, the numerical simulations carried out in reference [10] show that two hot spots do not interact between each other whenever the inequality $d/D > 0.15/[\nu_{iaw}/\omega_{iaw}]$ is fulfilled. For our experimental parameters, ν_{iaw}/ω_{iaw} can be estimated to be in the range 0.07–0.1 [12], so that one expects from these estimates,that the two hot spots interact whenever their mutual distance d satisfies $d < 18$–26 μm.

Concerning now the agreement between our experimental results with these estimates, we have already stated that Figure 2b demonstrates that the two neighboring hot spots strongly interact between each other when their mutual distance is $d = 20$ μm. On the other hand, the results corresponding to the inter-hot spot distance $d = 40$ μm, (not displayed here) do not show any significant interaction between the two hot spots: the transverse intensity distribution in the case of two hot spots appears to be the simple sum of the intensity distributions of two isolated hot spots, each intensity distribution behaving as previously described for a single hot spot. In conclusion, our experimental results do support the conjecture and the results obtained in reference [10] along which two neighboring hot spots of diameter D strongly interact between each other whenever their mutual distance d satisfies the condition $d/D < 0.15/[\nu_{iaw}/\omega_{iaw}]$, and do not interact otherwise.

We will end this section with a few comments concerning the thin exploded foil case "c". The corresponding image in Figure 1c does not allow to identify two separated hot spots, so that this case is strikingly different from the preformed-plasma case "b". The interaction, in the case of an exploding foil, involves processes that are more complex than in the preformed plasma case, namely ionization dynamics and electron waves, occurring on a fast time scale. Also, the IAW damping rate can be much weaker, leading to a significant change of the hydrodynamic-type interaction between neighboring hot spots, as compared with the preformed plasma experiments. More detailed experimental results and comparison with numerical simulations will be published in a forthcoming paper.

3 Space and time evolution of stimulated Brillouin scattering (SBS)

The second type of experiment was designed to study the spatial intensity distribution of stimulated Brillouin scattering (SBS) inside the plasma in the case of a RPP irradiation. To do so, a new imaging diagnostic was developed, which makes it possible to record 2D images of the SBS emission corresponding to a temporal integration of 100 ps at various times during the laser pulse. It enables us to compare the incident and back reflected spatial intensity distributions.

This second type of experiment was carried out on the LULI six beam facility. The laser beams were used with the same temporal pulse shape, but with different timings and colors. The pulse shape is close to Gaussian, the FWHM being in the order of 600 ps; however it differs from Gaussian, because the maximum intensity actually takes place at approximately 100 ps before mid-time of a Gaussian 600 ps FWHM Gaussian pulse. The interested reader is referred to reference [13] for the detailed characterization of the laser pulse shape. The two first beams were shot at 2ω on a thin plastic foil to produce a plasma, and the plasma was heated by a third 0.53 μm beam delayed by 1.1 ns; the interacting beam was the fourth beam, at 1.053 μm. A fifth beam was used at 0.35 μm, synchronized with the interaction beam, to probe by Thomson scattering the plasma parameters and the plasma waves associated with SBS. Random Phases Plates were used on all the beams in order to ensure a good reproducibility of the shots. The maximum intensity of the interaction beam was 8.5×10^{13} W/cm^2.

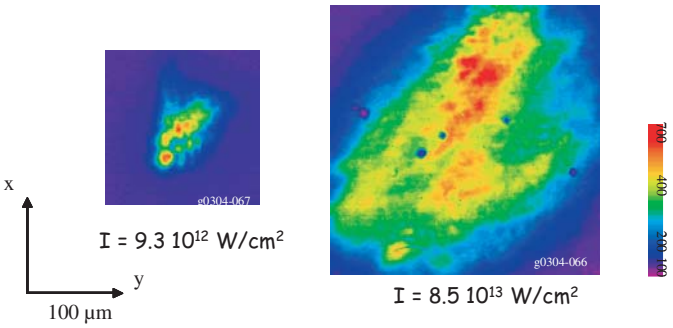

Fig. 3. (Colour online) Colour scaled transverse images of the SBS backscattered light intensity taken in the focal plane for two intensities of the incident RPP laser beam.

Results concerning the plasma parameters and the initial studies on SBS have been reported in previous publications [13,14]. Here we will simply summarize the new SBS features discussed in reference [15], and we will essentially focus on their modeling and numerical simulations. The main new SBS experimental results consisted in the demonstration that, for this combination of parameters, SBS was in a non-saturated regime. In particular, the plasma SBS active volume was observed to increase nonlinearly with the laser intensity, and the duration of the SBS activity was found to increase with the laser intensity. Concerning the plasma SBS active volume,

(i) we were able to measure its transverse area thanks to our imaging diagnostics. Two transverse images of the SBS backscattered light intensity, taken in the focal plane, are shown in Figure 3 for the laser intensities $I = 9.3 \times 10^{12}$ W/cm^2 and $I = 8.5 \times 10^{13}$ W/cm^2. These images correspond to a temporal integration of 100 ps and they were recorded at the time of maximum SBS emission. A strong increase of the emitting area can be clearly observed with increasing laser intensity;

(ii) the longitudinal extension of the SBS active volume has been deduced from the 3ω Thomson scattering diagnostic. The SBS-driven IAW waves were observed to be located in the front part of the plasma, and a clear increase of their longitudinal extension with

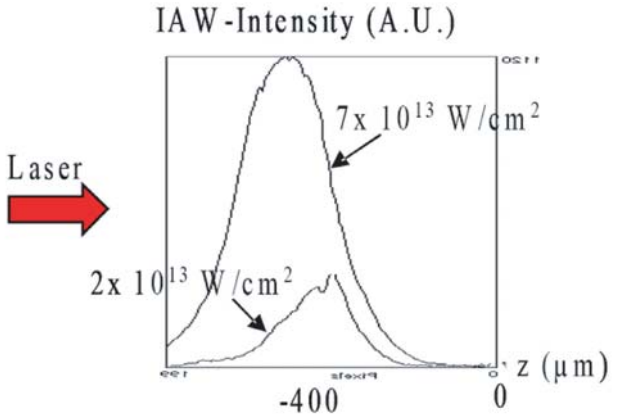

Fig. 4. Evolution of Thomson scattered intensity off the SBS-driven IAW as a function of the longitudinal coordinate z for the laser intensities $I = 2 \times 10^{13}$ W/cm^2 and $I = I = 7 \times 10^{13}$ W/cm^2.

increasing intensity was measured, as can be seen in Figure 4 showing the Thomson scattered intensity as a function of the longitudinal direction z for the two laser intensities $I = 2 \times 10^{13}$ W/cm^2 and $I = 7 \times 10^{13}$ W/cm^2.

All these results show that SBS was in an unsaturated regime in this RPP interaction beam experiment. Another evidence of SBS being in an unsaturated regime is that a modest increase of the intensity led to a larger increase of the reflectivity. Thus, the SBS reflectivity R jumped from $R = 0.1\%$ for $I = 2.5 \times 10^{13}$ W/cm^2 to $R = 1.05\%$ for $I = 8 \times 10^{13}$ W/cm^2. The origin of this SBS reflectivity increase can be detailed as being due to: (i) an increase of the transverse area $\Delta x \Delta y$ by a factor 4; (ii) an increase of the longitudinal extension Δz of the SBS-active region by a factor 1.5, and, (iii) an increase of the temporal duration Δt by a factor 2.

We now focus on the modeling of these experimental results. The numerical simulations were carried out with our code Harmony2D. The detailed description of this code can be found in references [13,16], so that we will simply summarize its main features. The calculations with Harmony2D are based on the decomposition into various spatial scales, allowing for an efficient computation of the different quantities describing the plasma [16,17]: the plasma expansion (long-wavelength) is described by an usual hydrodynamics code, whereas the IAW excited by the instabilities (short-wavelength) are described by envelope equations. The IAW nonlinearities can be taken into account by solving additional equations describing the IAW harmonics and sub-harmonics. The total transverse electric field is decomposed in a forward and a backward component, for each of which the paraxial approximation is made. The momentum transfer into the flow caused by the IAW excitation due to the SBS instability is also taken into account [17].

The numerical results with Harmony2D in 2 spatial dimensions reproduce nicely the experimental features of the SBS-driven IAWs, in particular, the localization of

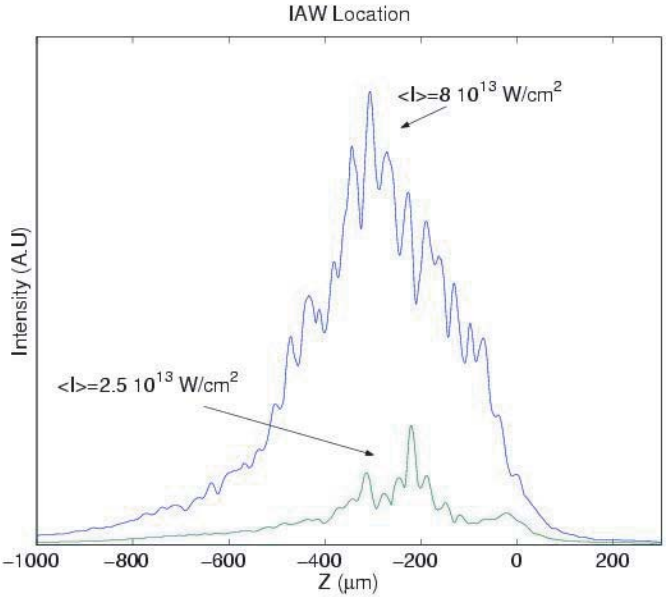

Fig. 5. Amplitude of the SBS-driven IAW obtained from Harmony2D simulations, for the two laser intensities $\langle I \rangle = 2.5 \times 10^{13}$ W/cm^2 and $\langle I \rangle = 8 \times 10^{13}$ W/cm^2. The maximum IAW relative amplitude is $\delta n/n \approx 1.6 \times 10^{-2}$ in the case $\langle I \rangle = 2.5 \times 10^{13}$ W/cm^2, and $\delta n/n \approx 6 \times 10^{-2}$ in the case $\langle I \rangle = 8 \times 10^{13}$ W/cm^2.

the IAW in the front part of the plasma, and the increase of the SBS activity area with the laser intensity increase. Figure 5 shows the amplitude of the SBS-driven IAW obtained from Harmony2D simulations, for the two laser intensities $\langle I \rangle = 2.5 \times 10^{13}$ W/cm^2 and $\langle I \rangle = 8 \times 10^{13}$ W/cm^2. The maximum IAW relative amplitude $\delta n/n$ is $\delta n/n \approx 4 \times 10^{-3}$ in the case $\langle I \rangle = 2.5 \times 10^{13}$ W/cm^2, and $\delta n/n \approx 1.4 \times 10^{-2}$ in the case $\langle I \rangle = 8 \times 10^{13}$ W/cm^2. These two numerically simulated IAW profiles can be observed to be close to the experimental Thomson scattered intensity profiles displayed in Figure 4.

In order to properly compare the simulation results with the experimental ones, the numerical simulations averaged SBS reflectivity, denoted as $\langle R \rangle$, was computed by integrating in time over the backscattered light collected in the same aperture angle as the one of the incident light beam, in order to reproduce the experimental conditions. The values are then found to be very close to the experimental reflectivities: thus, for $\langle I \rangle = 8 \times 10^{13}$ W/cm^2, the numerical simulations lead to the SBS reflectivity $\langle R \rangle = 1.5\%$, when the experimental SBS reflectivity R_{exp} was $R_{exp} \sim 1\%$. It is interesting to point out that this low reflectivity does not result from nonlinear saturation mechanisms. Indeed, we compared the results from (i) simulations in which we retained the IAW nonlinearities corresponding to harmonics and sub-harmonics generation, together with a nonlinear frequency shift modeling kinetic effects, with (ii) those in which we completely ignored the IAW nonlinearities. We did not see any significant differences concerning the mean reflectivity, although the instantaneous SBS reflectivity could attain short-time peak

values as high as 20–40% in the case where no IAW nonlinearity was kept. Such high transient reflectivity values were reached during short time intervals, of the order of a few ps. Thus, we conclude that in the parameter regime of these experiments, the IAW nonlinearities do not play a major role, and that the low value of the averaged reflectivity $\langle R \rangle$ is due to (i) the spatial and temporal incoherence induced by plasma-smoothing [2] in the most intense speckles; and (ii) the fact that the plasma density decreases with time on the time scale of the laser pulse, resulting in a decrease of the SBS growth rate. On the other hand, we found that the proper characterization of the plasma density profile and of the temperatures (before starting the simulations with the interaction beam) has to be carried out accurately. Similarly, we found it very important to take into account collisional and nonlocal transport effects [18] during the laser-plasma interaction, to quantitatively reproduce the experimental results by numerical simulations. More recently, in a work still in progress and concerning LULI monospeckle experiments, we found similarly a very good agreement between the experimental results and our Harmony2D simulations. The mean reflectivity was observed to be low as well, and in this case of a monospeckle experiment the low reflectivity value was interpreted as being due to the onset of the filamentation instability [2]. This instability leads to the reduction of the spatial coherence of the monospeckle, so that SBS grows to levels that are much below the predictions based on the spatial amplification of a coherent laser beam.

4 Conclusion

After many years of efforts, important progresses have been achieved, both in the experiments and in the numerical modeling. These combined progresses now allow to compare experimental and simulation results on a quantitative level. Thus, well diagnosed experiments, carried out with well defined laser beam and plasma conditions, make it possible to benchmark our theoretical and numerical modeling, and hence, to improve our predictive capabilities. In the work presented here, we have experimentally demonstrated the interaction between hot spots for the first time, in accordance with theoretical predictions. Furthermore, for the case of mm-size expanding plasmas, numerical simulations involving SBS backscattering have shown very close agreement with the experiments. In this unsaturated regime, the non local transport reveals to be an important feature to reproduce the low lSBS reflectivity values.

References

1. W.L. Kruer, *The Physics of Laser Plasma Interactions* (Addison Wesley, Redwood City, CA, 1988); H.A. Baldis, E.M. Campbell, W.L. Kruer, Laser-Plasma Interactions, in *Physics of Laser Plasmas*, Handbook of Plasma Physics (North-Holland, Amsterdam, 1991), pp. 361–434; D. Pesme, C. Labaune, *La Fusion Thermonucléaire Inertielle par Laser* (Eyrolles, Paris, 1993), Vol. 1
2. D. Pesme, W. Rozmus, V.T. Tikhonchuk, A. Maximov, I. Ourdev, C.H. Still, Phys. Rev. Lett. **84**, 278 (2000); P. Michel, C. Labaune, S. Weber, V.T. Tikhonchuk, G. Bonnaud, G. Riazuelo, F. Walraet, Phys. Plasmas **10**, 3545 (2003)
3. W.L. Lindl, Phys. Plasmas **2**, 3933 (1995)
4. J.L. Kline et al., J. Phys. IV France **133**, 919 (2006); J.C. Fernandez et al., Phys. Plasmas **13**, 056319 (2006)
5. K. Lewis, G. Riazuelo, C. Labaune, Rev. Sci. Instrum. **76**, 093502 (2005)
6. Y. Kato, K. Mima, N. Miyanaga, S. Arinaga, Y. Kitagawa, M. Nakatsuka, C. Yamanaka, Phys. Rev. Lett. **53**, 1057 (1984); A. Schmitt, Phys. Fluids **31**, 3079 (1988)
7. D. Montgomery, R. Johnson, J. Cobble, J. Fernandez, E. Lindman, H. Rose, K. Estabrook, Laser Part. Beams **17**, 349 (1999); D.S. Montgomery, R.P. Johnson, H.A. Rose, J.A. Cobble, J.C. Fernández, Phys. Rev. Lett. **84**, 678 (2000)
8. H.A. Rose, D.F. DuBois, Phys. Fluids B **5**, 590 (1993); H.A. Rose, D.F. DuBois, Phys. Rev. Lett. **72**, 2833 (1994)
9. V.T. Tikhonchuk, C. Labaune, H.A. Baldis, Phys. Plasmas **3**, 3777 (1996); S. Hüller, Ph. Mounaix, V.T. Tikhonchuk, Phys. Plasmas **5**, 2706 (1998); V.T. Tikhonchuk, J. Fuchs, C. Labaune, S. Depierreux, S. Hüller, J. Myatt, H. Baldis, Phys. Plasmas **8**, 1636 (2001)
10. S. Hüller, P. Mounaix, V.T. Tikhonchuk, D. Pesme, Phys. Plasmas **4**, 2670 (1997)
11. This criterion is based, for simplicity, on plane geometry, while cylindrical or spherical geometry will lead to even faster attenuation
12. M. Casanova, Laser Part. Beams **7**, 165 (1989)
13. P.-E. Masson-Laborde, S. Hüller, D. Pesme, M. Casanova, P. Loiseau, J. Phys. IV France **133**, 247 (2006)
14. C. Labaune, H.A. Baldis, N. Renard, E. Schifano, A. Michard, Phys. Rev. Lett. **76**, 3727 (1996)
15. C. Labaune, K. Lewis, H. Bandulet, S. Depierreux, S. Hüller, P.-E. Masson-Laborde, D. Pesme, G. Riazuelo, J. Phys. IV France **133**, 29 (2006)
16. S. Hüller, P.E. Masson-Laborde, D. Pesme, M. Casanova, F. Detering, A. Maximov, Phys. Plasmas **13**, 022703 (2006)
17. D. Pesme, S. Hüller, J. Myatt, C. Riconda, A. Maximov, V.T. Tikhonchuk, C. Labaune, J. Fuchs, S. Depierreux, H.A. Baldis, Plasma Phys. Contr. Fusion **44**, B53 (2002)
18. A.V. Brantov, V.Yu. Bychenkov, V.T. Tikhonchuk, W. Rozmus, Phys. Plasmas **5**, 2742 (1998)